

# **Geometrical corrections for poststack image focusing velocity analysis**

Adrian D. Smith and Robert J. Ferguson

## **ABSTRACT**

Knowing the subsurface velocity structure is crucial in generating accurate images from geophysical reflection data. Velocity information commonly comes from moveout analysis on shot and/or CMP gathers in seismic reflection surveys. In cases where we do not have offset information such as fixed-offset georadar (GPR) surveys, we can collapse diffractions in the data through migration to obtain velocities. However, there are a number of reflection geometries where the reflection signature appears hyperbolic in shape similar to that of a point diffractor. Collapsing such hyperbolic events gives inaccurate velocity information. We investigate three geometrical cases where this may occur: circular, hyperbolic, and parabolic. We derive zero-offset traveltime equations for each case assuming a homogeneous media between the ground surface and reflector. Generating a randomly distributed set of diffractors over a range of depths and medium velocities at georadar scale, we use a grid-search method to determine the best-fitting parameters for each of the geometric cases. We find that in all three cases, observed diffractor velocities are always lower than the "true" medium velocities, and in the circular and parabolic cases we are able to estimate a crude velocity factor relying only on an estimate of one scale parameter. We apply a velocity correction to a georadar dataset with circular culverts and show that it gives a more accurate final image than using just a diffractor velocity. In the future we would like to improve our inversion strategy as well as extend the traveltime derivation to a fixed-offset case.

## **INTRODUCTION**

Proper imaging of geophysical reflection data such as seismic or georadar (GPR) requires knowledge of the velocity of subsurface materials in order to place reflection events in their proper locations. Collecting multi-offset data usually provides a means to obtain velocity information by some type of moveout analysis, making the assumptions that the Earth is locally laterally homogeneous and reflectors are horizontal (Yilmaz, 2001).

We have to use other methods to obtain velocity information when we do not have offset information. Such cases include poststack seismic data where stacking removes offset information, and georadar (GPR) data which is commonly acquired at fixed offset. Georadar imaging is often performed assuming a very simplified velocity field such as constant velocity which gives only approximate subsurface images. Usually, heterogeneity and anisotropic factors are unaccounted for (Forte et al., 2014). Other non-moveout based velocity analysis methods have been proposed such as in (Forte et al., 2014), whereby velocities are estimated from inverting reflection amplitudes to compute a series of reflection coefficients. These are in turn used to estimate the velocity in each interpreted layer. With a lack of specular reflections, we can estimate velocities in common-offset georadar sections by taking into account diffracted events. This method is motivated by the fact that georadar energy is partly scattered when the subsurface contains objects having size smaller than its

mean wavelength (Grasmueck et al., 2005). Point diffractors give hyperbolic reflection signatures on a common-offset georadar section and by fitting analytic curves corresponding to different-velocity media we obtain velocity estimates (Novais et al., 2008). This process is referred to as "Diffraction hyperbola fitting" (Forte et al., 2014).

A significant issue with diffraction hyperbola fitting arises when observed events are a combination of reflection and diffraction energy, especially where reflection energy comes from curved interfaces (Forte et al., 2014). Diffraction hyperbola fitting in these circumstances results in incorrect velocity estimations. Biondi (2009a) and Biondi (2009b) attempt to remove the ambiguity velocity and reflector curvature by introducing a curvature correction into the computation of a semblance functional that estimates image coherency (and hence velocities).

### Houston Coastal Centre georadar dataset

This work is motivated in part by a georadar dataset acquired over a series of culverts at the Houston Coastal Centre (Figure 1). These culverts generate a series of hyperbolic reflection signatures (Figure 2). de Figueiredo et al. (2011) and de Figueiredo et al. (2013) use this dataset to test a kNN classifier to detect diffractions in common-offset gathers. It is successful at identifying four "diffractors", which are located at the apex of each culvert. The hyperbolic signatures in this dataset are very pronounced, and it proves an excellent dataset with which to test the classification. However, their hyperbola diffraction-fitted velocity assumes a point diffractor origin and not a specular reflection from the circumference of the culverts.

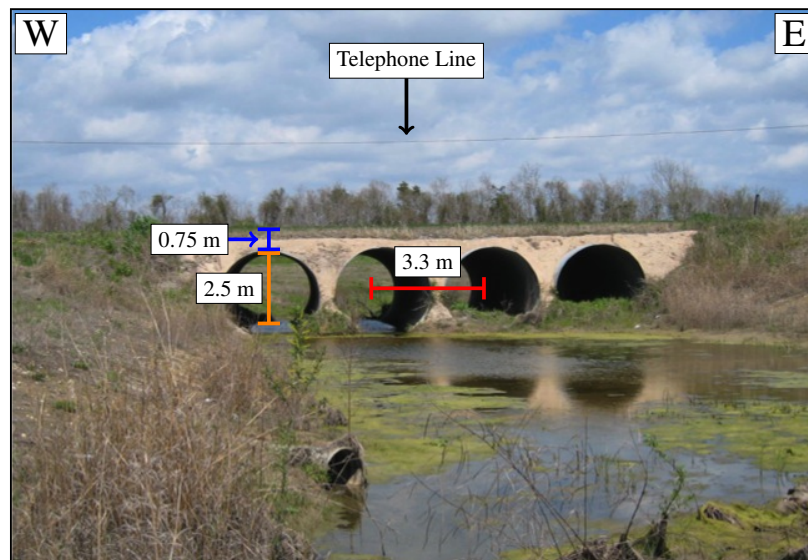


FIG. 1. Cross-sectional view of the culverts at the Houston Coastal Center, targeted by a georadar (GPR) survey (Smith et al., 2014).

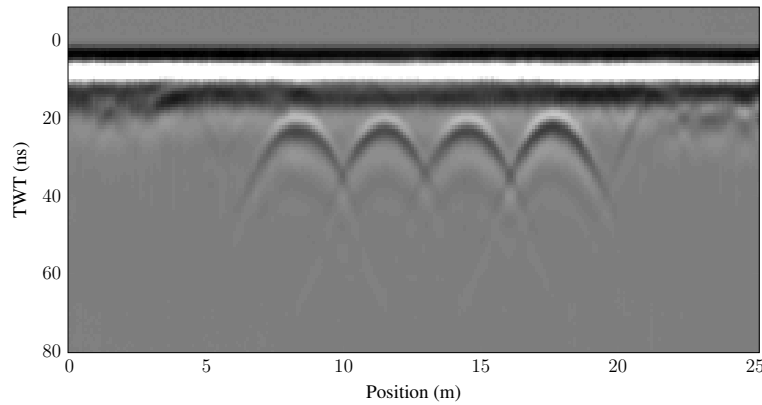


FIG. 2. Raw unprocessed 2D georadar line from Smith et al. (2014), illustrating the hyperbolic-like signature of the reflections from the culverts in Figure 1.

In this case, we know that the true image is not a point diffractor, rather the reflected energy is coming from a specular reflector in a pattern that appears hyperbolic on the common-offset section. This leads to the problem that velocities obtained by diffraction hyperbola fitting will only be correct if the true geometry is a point diffractor. If we have some idea of what geometry our objects have then we can estimate a correct velocity to use for imaging that will not necessarily collapse hyperbolic signatures. We would like to determine a velocity correction based solely on observed diffractor velocities, but due to non-uniqueness it will also require some knowledge or assumption of a scale parameter of the object(s) under question.

Unlike the methods of Biondi (2009a) and Biondi (2009b) which make use of semblance calculations, we start with a theoretical description of traveltimes from various reflector geometries: point diffractor, circular interface, hyperbolic interface, and parabolic interface. Although image targets with near-perfect symmetries and curvatures rarely occur in natural settings, they may be present when georadar is used to investigate artificial structures or materials. We develop analytic expressions for zero-offset traveltimes for three geometric cases and use these to develop a velocity correction factor to apply to an observed diffractor velocity for two of the cases. We then apply such a correction to the 2D Culvert Line from the Houston Coastal Center.

## INTERFACE GEOMETRIES

In this section, we examine the geometries of the following interfaces giving rise to hyperbolic reflection events in zero-offset data: point diffractor, circle, hyperbola, and parabola. We derive equations that give the normal distance  $d$  from each type of reflection interface to a station located at some arbitrary location  $S(S_x, 0)$  on the surface. Assuming a constant medium velocity above the interface, we will be able to use this information to calculate traveltimes  $\tau$ .

## Point diffractor

We begin with a simple model of a point diffractor or scatterer in a constant-velocity homogeneous medium buried at some depth  $z_D$  in the subsurface (Figure 3a). When we observe symmetric reflection hyperbolae in zero-offset or stacked sections, we assume that they originate from point diffractors. Velocity analysis proceeds by focusing these diffractions. Thus, a brief understanding of their geometry is important.

We assume that the point scatterer is located at some point  $Q_d(0, z_D)$ . For point scatterers or diffractors in the subsurface, the relationship between horizontal distance or offset ( $x$ ) and normal distance from the scatterer to the station location  $d(x)$  is a simple right triangle (Figure 3b). This distance is given as

$$d(x) = d(S_x) = \sqrt{x^2 + z_D^2}, \quad (1)$$

where we take the positive square root because distance  $d(x)$  must be positive.

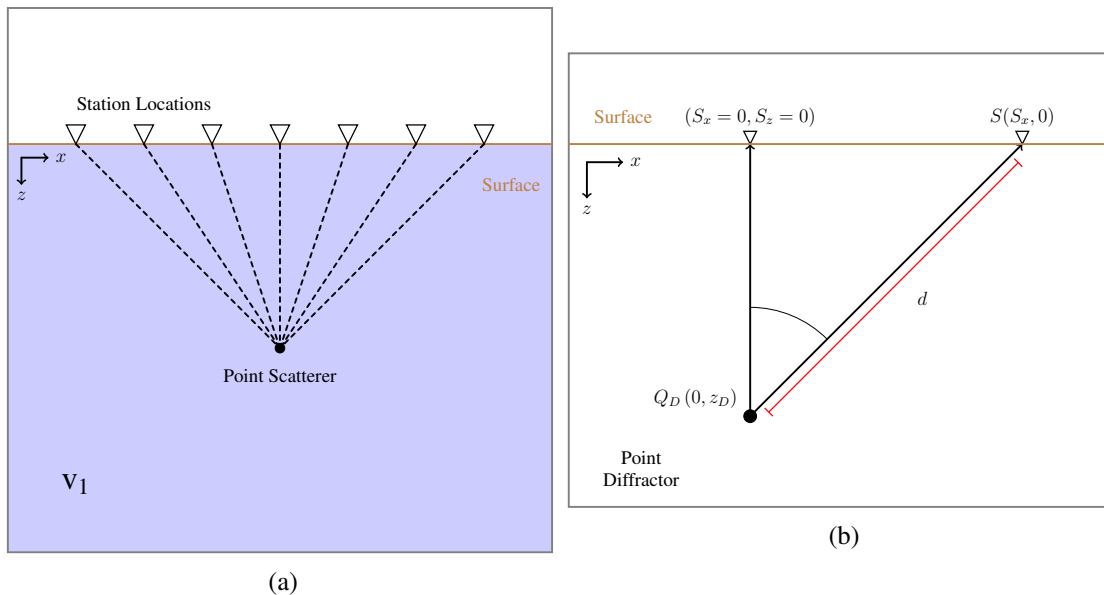


FIG. 3. Illustration of the geometry of the point diffractor problem. a) shows a representation of the raypaths from the scatterer to the stations in a zero-offset acquisition setting. b) gives the geometry of an individual raypath.

## Circular reflector

The first reflector geometry that we discuss is that of a buried circle. We assume a case where there is an increase in velocity from the medium above the circular interface  $v_1$ , to the velocity in the lower medium  $v_2$  (Figure 4a). A general equation of a circle in the  $x$ - $z$  plane with a radius of  $r$  and centre at  $(x_0, z_0)$  is given as

$$(x - x_0)^2 + (z - z_0)^2 = r^2. \quad (2)$$

We let  $x_0$  be equal to zero in order to simplify the geometry of the problem to being symmetric in the horizontal direction about the  $z$ -axis. We then rearrange the formula to describe the lower half of the circle, since our positive- $z$  axis is in the downward direction and we do not require the positive-signed square root. This gives the relation

$$z(x) = z_0 - \sqrt{r^2 - x^2}, \quad (3)$$

where  $|x| \leq r$ . In the case that we are located directly above the apex of the circle ( $x = 0$ ), we note that the relation reduces to  $z = z_0 - r$ . Therefore, we define  $z_T = z(x = 0) = z_0 - r$  to be equal to the vertical depth to the top of the circle, with the condition that  $z_T > 0$ , or  $z_0 > r$ . We want to find the distance  $d$  of a straight raypath travelling from a station location  $S(S_x, 0)$  to a reflection point on and normal to the curvature of the circle.

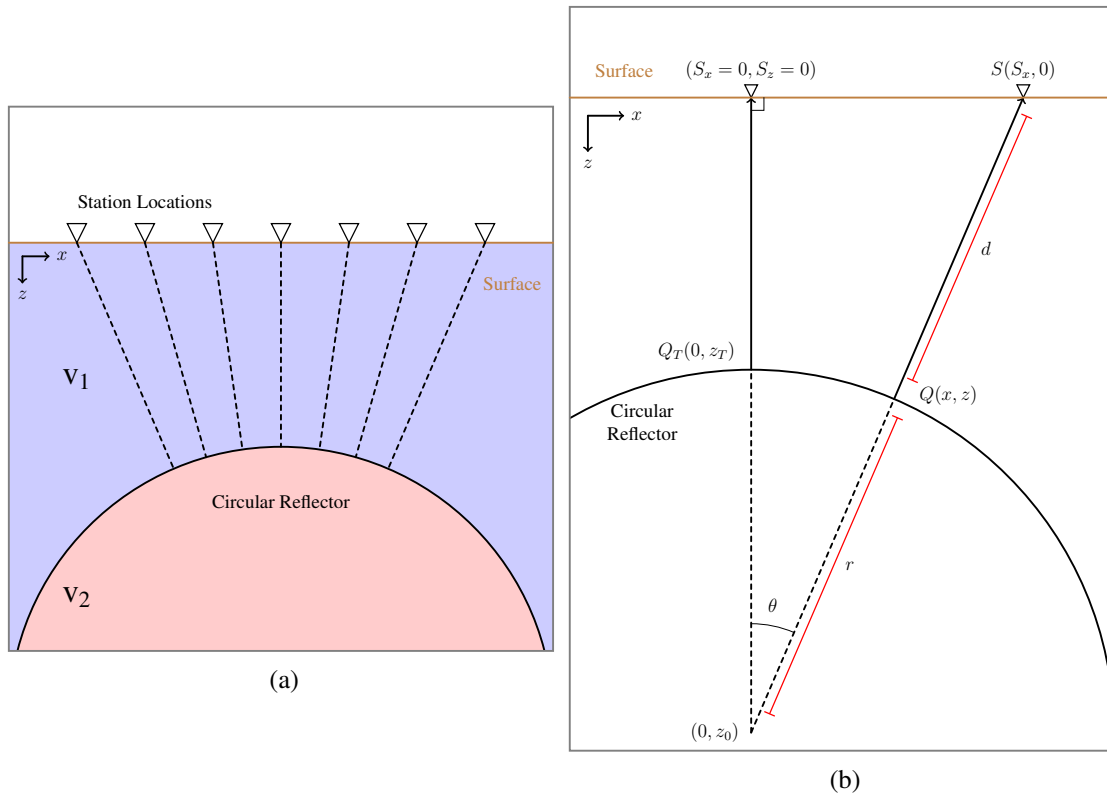


FIG. 4. Illustration of the geometry of the circular reflector problem. a) shows a representation of the raypaths from the reflector to the stations in a zero-offset acquisition setting. b) gives the geometry of an individual raypath.

Using the geometry as presented in Figure 4b, the problem is quite simple as any straight raypath travelling from the centre of the circle to a point outside it will always intersect the circumference normally. Using the large right triangle in Figure 4b, we get

$$(r + d)^2 = S_x^2 + z_0^2. \quad (4)$$

Rerranging this for  $d$ , we get the following relation for distance

$$d(S_x) = d(x) = \sqrt{x^2 + z_0^2} - r. \quad (5)$$

Note the coordinate systems.  $S_x$  is defined for any point on the surface of the Earth  $[-\infty \infty]$  (in theory since any surface point should receive reflection energy), while the range of  $x$  is governed by the geometry of the circle and is bounded by the condition  $|x| \leq r$  (in the case of the circle).

### Hyperbolic interface

Another obvious case for an alternative reflector interface geometry giving rise to a specular hyperbolic reflection signature on zero-offset reflection data is that of a physical hyperbola in the subsurface (Figure 5).

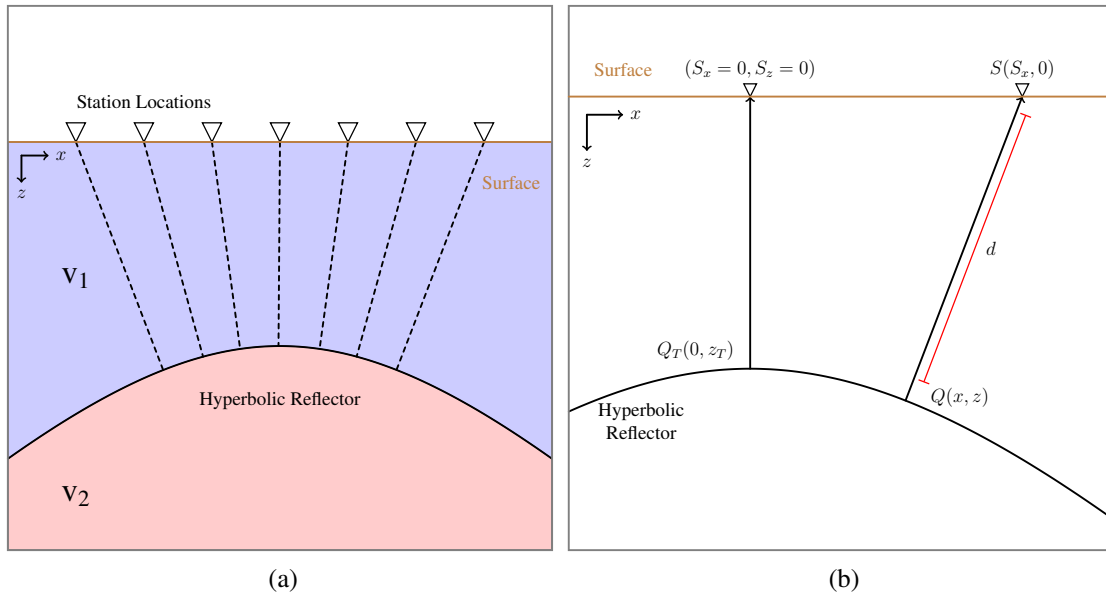


FIG. 5. Illustration of the geometry of the hyperbolic interface situation. a) shows a representation of the raypaths from the reflector to the stations in a zero-offset acquisition setting. b) gives the geometry of an individual raypath.

We assume a simple case such as in Figure 5a where there is an increase in velocity from the medium above a concave-down hyperbolic interface  $v_1$ , and a faster velocity in the lower medium  $v_2$ , generating a specular reflection. A general equation of a hyperbola in the  $x$ - $z$  domain with the transverse axis aligned with the  $z$ -axis, opening "Up-Down" is given as

$$\frac{(z - z_0)^2}{a^2} - \frac{(x - x_0)^2}{b^2} = 1, \quad (6)$$

where  $x_0$  and  $z_0$  are the respective horizontal and vertical shifts of the central point of the hyperbola. We let  $x_0$  be equal to zero in order to simplify the geometry of the problem to being symmetric in the horizontal direction about the  $z$ -axis. We then rearrange the formula to describe the upper branch of the hyperbola, since our positive- $z$  axis is in the downward direction and we do not require the negative-signed square root. This gives

$$z(x) = a\sqrt{1 + \frac{x^2}{b^2}} + z_0, \quad (7)$$

where the parameters  $a$  and  $b$  describe the curvature of the hyperbola. In the case that we are located directly above the apex of the hyperbola ( $x = 0$ ), we note that the relation reduces to  $z = a + z_0$ . Therefore, we define  $z_T = z(x = 0) = a + z_0$  to be equal to the vertical depth to the top of the hyperbola, with the condition that  $z_T > 0$ , or  $a > -z_0$ . We want to find the distance  $d$  of a straight raypath travelling from a station location  $S(S_x, 0)$  to a reflection point on and normal to the curvature of the hyperbola at point  $Q(x, z)$  (Figure 5b).

The manner in which we calculate this is as follows. First, find the tangent and normal slopes for each point on the hyperbola. Next, we use the basic form of a 2-D line in the  $x$ - $z$  domain to calculate the location of each station  $S(S_x, 0)$  that corresponds with a normal reflected ray for every point on the hyperbola  $Q(x, z)$ . Using this information, we can calculate the distance from  $S$  to  $Q$ , giving us the normal reflection distance.

First, we calculate the value of the tangent of every point along the hyperbola using equation 7 as a starting point

$$\frac{d}{dx}z(x) = \frac{dz}{dx} = \left(\frac{a}{b^2}\right)x \left(1 + \frac{x^2}{b^2}\right)^{-1/2}. \quad (8)$$

From this, the slope of the line normal to the hyperbolic reflector is

$$m(x) = -\frac{dx}{dz} = -\left(\frac{b^2}{a}\right)\left(\frac{1}{x}\right)\left(1 + \frac{x^2}{b^2}\right)^{1/2}, \quad (9)$$

which comes from the negative reciprocal rule for perpendicular lines. Next, we define a straight line running from  $Q$  to  $S$  as

$$z = mx + c, \quad (10)$$

where  $z$ ,  $m$ , and  $c$  are all functions of  $x$ . We now can substitute in the points  $Q$  and  $S$  as well as  $m$  from equation 9 into 10 to determine the form of  $c$ . We begin with with substituting in the point  $Q(x, z)$  into 10 to get the following expression for  $c$

$$\begin{aligned} z &= mx + c \\ [z] &= \left[ - \left( \frac{b^2}{a} \right) \left( \frac{1}{x} \right) \left( 1 + \frac{x^2}{b^2} \right)^{1/2} \right] (x) + c \\ c &= z + \left( \frac{b^2}{a} \right) \left( 1 + \frac{x^2}{b^2} \right)^{1/2}. \end{aligned} \quad (11)$$

We now substitute the point  $S(S_x, 0)$  into 10 along with the expressions for  $m$  and  $c$  from equations 9 and 11 respectively to get

$$\begin{aligned} [S_z] &= m [S_x] + c \\ (0) &= - \left( \frac{b^2}{a} \right) \left( \frac{1}{x} \right) \left( 1 + \frac{x^2}{b^2} \right)^{1/2} S_x + z + \left( \frac{b^2}{a} \right) \left( 1 + \frac{x^2}{b^2} \right)^{1/2}. \end{aligned} \quad (12)$$

We now rearrange 12 for  $S_x$  and substitute in the expression for  $z$  from equation 7 to get a relationship for  $S_x$  in terms of  $x$

$$\begin{aligned} S_x(x) &= z \left( \frac{a}{b^2} \right) x \left( 1 + \frac{x^2}{b^2} \right)^{-1/2} + x \\ &= \left[ a \left( 1 + \frac{x^2}{b^2} \right)^{1/2} + z_0 \right] \left( \left( \frac{a}{b^2} \right) x \left( 1 + \frac{x^2}{b^2} \right)^{-1/2} \right) + x \\ &= x \left( \frac{a^2}{b^2} + \frac{z_0 a}{b^2} \left( 1 + \frac{x^2}{b^2} \right)^{-1/2} + 1 \right) \end{aligned} \quad (13)$$

Now that we have an expression for the  $S_x$  in terms of  $x$ , we can calculate the distance from  $Q$  to  $S$  as

$$\begin{aligned} d(x) &= \sqrt{(S_x - x)^2 + (0 - z)^2} \\ &= \sqrt{(S_x - x)^2 + z^2}, \end{aligned} \quad (14)$$

where again, both  $z$  and  $S_x$  are in terms of  $x$  as given in equations 7 and 13 respectively. This relationship is in terms of  $x$ , not in  $S_x$ . Rearranging 14 in terms of  $S_x$  is non-trivial and in order to get  $d(S_x)$ , we interpolate the values using  $S_x(x)$  as a guide.

## Parabolic geometry

The final conic form giving rise to a hyperbolic reflection discussed here is that of a downward opening parabola (Figure 6). Similar to the hyperbolic interface case, we have an increase in medium velocity giving rise to a specular reflection 6a. Our derivation of  $d(x)$  is very similar as in the hyperbolic case discussed previously.

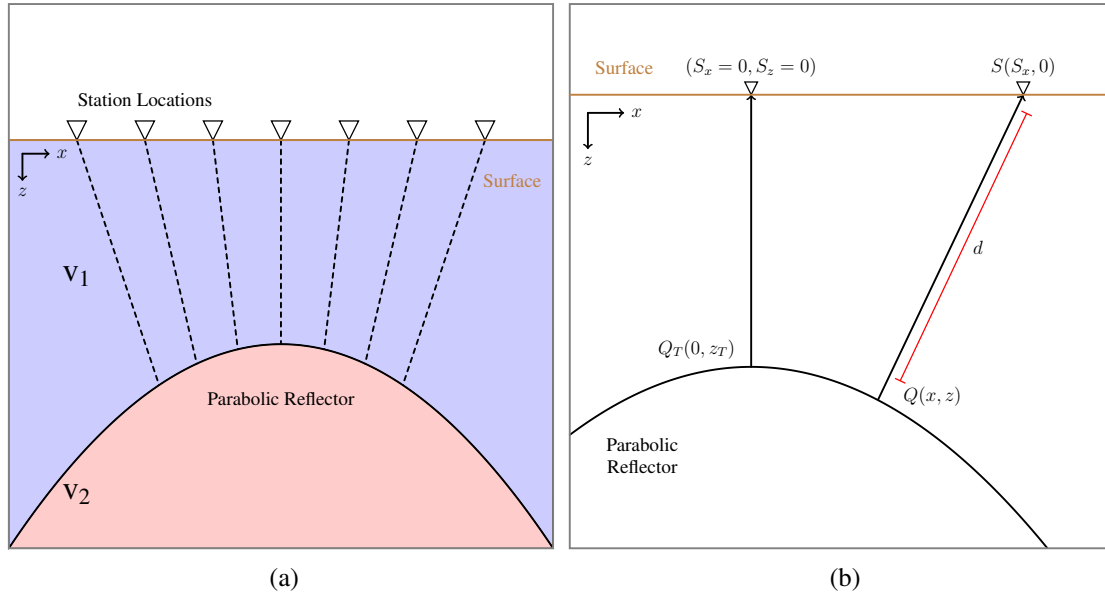


FIG. 6. Illustration of the geometry of the parabolic interface situation. a) shows a representation of the raypaths from the reflector to the stations in a zero-offset acquisition setting. b) gives the geometry of an individual raypath.

The general form of a parabola is

$$(x - x_0)^2 = 4p(z - z_0), \quad (15)$$

where  $(x_0, z_0)$  is the location of the vertex of the parabola and  $p$  is a parameter that uniquely defines the curvature of a parabola. Similar to the cases of the circle and hyperbola, we set  $x_0$  equal to zero, rearrange for depth, and the relation becomes

$$z(x) = \frac{x^2}{4p} + z_0. \quad (16)$$

Again, we say that the vertex of the parabola (apex of the curve) is located at  $z_0 = z_T$ . Although  $p$  can be negative, it can only be for small values as  $-z_0 < \frac{x^2}{4p} < 0$ , since our depth is positive and the vertex is buried beneath the surface.  $p$  also cannot equal 0. The only parameter that affects the shape of the interface is  $p$ . Since  $z_0 = z_T$ , changes in  $z_0$  only result in vertical shifts, and do not affect the curvature of the parabola.

The slope of the line normal to the parabolic reflector is

$$m(x) = -\frac{dx}{dz} = -\frac{4p}{x}. \quad (17)$$

Following a similar process to that in section , we calculate  $S_x$  as a function of  $x$ , which gives a result of

$$S_x = x \left( \frac{x^2}{16p^2} + \frac{z_0}{4p} + 1 \right). \quad (18)$$

Using our expressions for  $z$  and  $S_x$  from equations 16 and 18, we calculate the distance from  $Q$  to  $S$  using equation 14

$$d(x) = \sqrt{(S_x - x)^2 + z^2}. \quad (19)$$

where again, as in the hyperbolic case, we need to appropriately interpolate the result of  $d(x)$  in order to get  $d(S_x)$ .

### VELOCITY CORRECTION

We use the distance formulae obtained in equations 1, 5, 14, and 19 to compare their traveltimes on a zero-offset section. We use a grid-search inversion to determine the errors in velocity estimation introduced by different geometries as well as derive velocity correction factors.

In Figure 7 we illustrate various reflector geometries and in Figure 8 we illustrate the normal raypath distance from the reflector to each station location on an interval  $-10 \leq S_x \leq 10$ . In these examples, the diffractor depth  $z_D$  is set at 2 m and is equal to the apex  $z_T$  of each of the other geometries. In the circular case, the centre of the circle is located at a depth  $z_0$  of 7 m, with a radius  $r$  of 5 m. In the hyperbolic case,  $a$  and  $b$  are both equal to two, and  $z_0$  is equal to zero. In the parabolic case,  $p$  is equal to two.

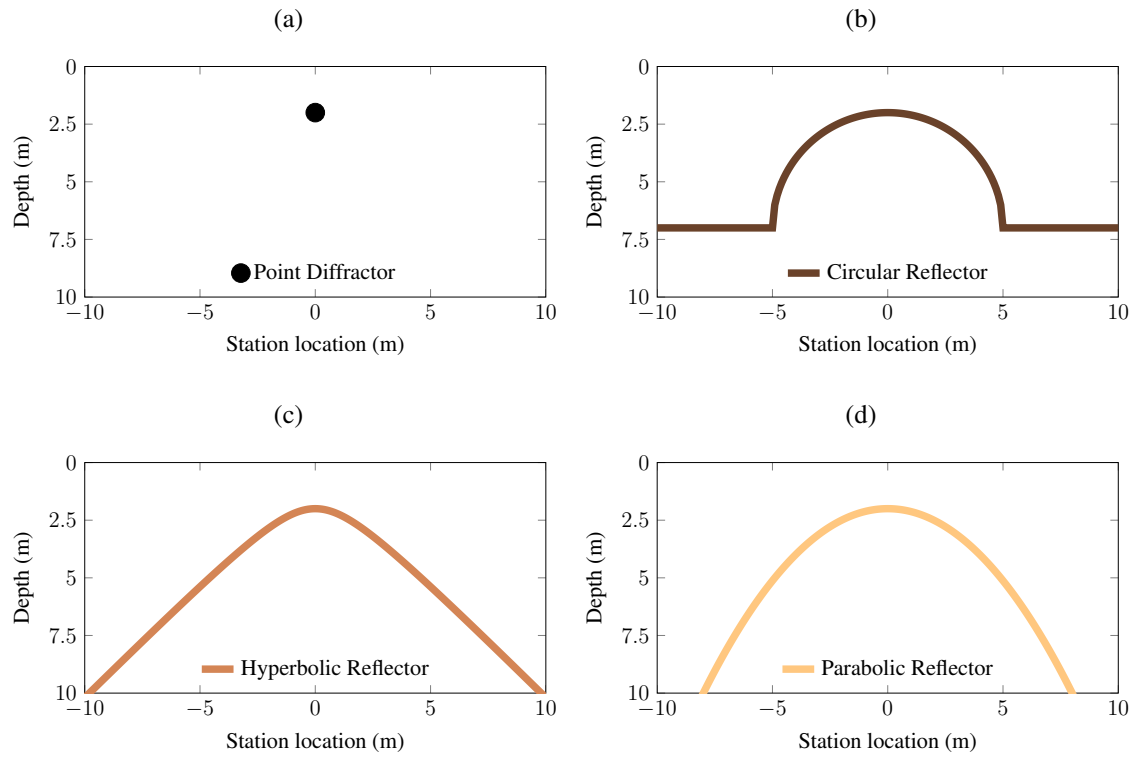


FIG. 7. Illustration of reflector geometry for 4 different cases: (a) - point diffractor buried at 2 m, (b) - circular reflector, (c) - hyperbolic reflector, and (d) - parabolic reflector

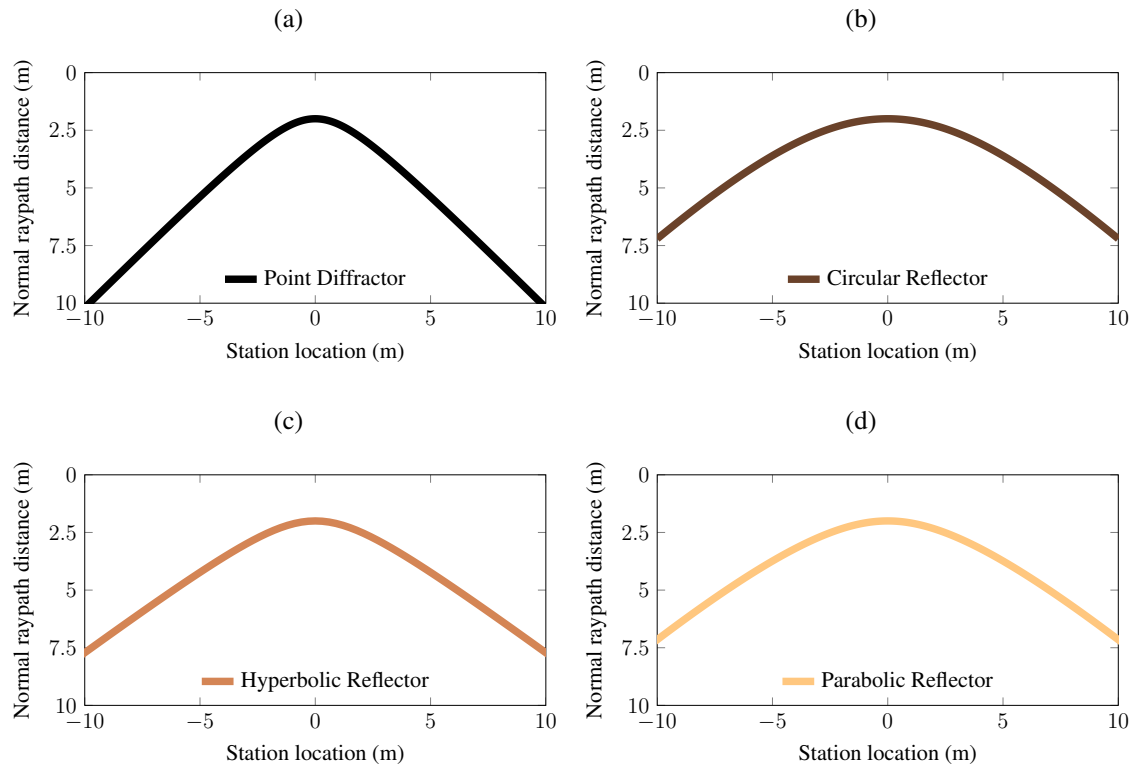


FIG. 8. Illustration of reflector geometry for four different cases: (a) - point diffractor buried at 2 m, (b) - circular reflector, (c) - hyperbolic reflector, and (d) - parabolic reflector

Using a velocity of 30% of the speed of light ( $c \approx 2.9979\text{m/s}$ ) and the zero-offset distances from Figures 8a-d), we generate two-way traveltimes for zero-offset reflections for each of the four geometric cases in Figures 7a-d) (Figure 9).

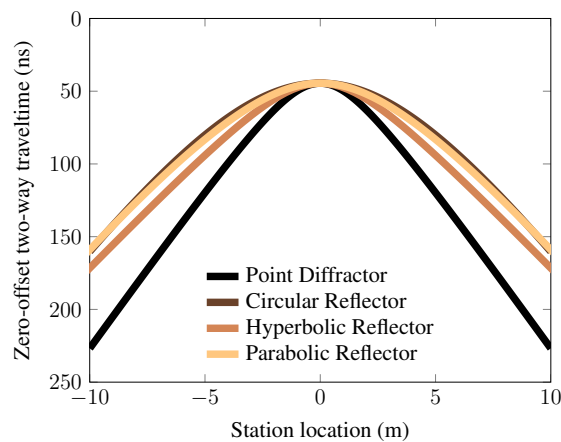


FIG. 9. Illustration of two-way traveltimes from zero-offset reflections for the four different geometric cases in figures 7a-d).

Looking at the curves in Figure 9, we see that the three non-point diffractor cases give

traveltime curves that are very similar to one another although they come from different geometries. This describes the ambiguity in reflector geometry that we are trying to address. The traveltime curve is the only piece of information that we have when looking at zero-offset data. In traditional analysis, we assume a point diffractor case and estimate the velocity using diffraction hyperbola fitting. We want to estimate a velocity correction factor for non-diffractor geometries that can be applied to estimate a more accurate imaging velocity without any apriori information other than an assumption of geometry type. To accomplish this, we use a simple grid-search inversion.

### Grid-search inversion

In the point diffractor case, our two-way traveltime curve  $\tau_D = f(x, v_D, z_D)$  is a function of offset ( $x$ ), velocity ( $v_D$ ) and diffractor depth ( $z_D$ ). When we collapse diffractions on a zero-offset section, we are able to estimate  $v_D$  and  $z_D$  (assuming that the medium is homogeneous and we actually have a point diffractor geometry. In the non-diffractor geometries, the traveltime curves  $\tau_G = f(x, v_G, param)$ , where  $v_G$  generally does not equal  $v_D$  and  $param$  is a number of parameters that uniquely describe the geometry in depth (eg.  $z_0$  and  $r$  in the circular case). Our goal is to find the parameters  $v_G$  and  $param$  that make  $\tau_G$  fit the best with  $\tau_D$ . We can then estimate a velocity correction factor based on a comparison of  $v_G$  with  $v_D$ .

Our method is a simple grid-search inversion to find  $v_G$  and  $param$  implemented as follows:

- Assign a  $v_D$  and  $z_D$  within a specified range, and calculate  $\tau_D$ .
- Looping over a range of  $v_G$  and each parameter in  $param$ , calculate  $\tau_G$  and estimate a residual value  $\bar{\epsilon}$ . This residual is simply the normalized absolute difference of  $\tau_D$  and  $\tau_G$  for each iteration.
- Keep the values of  $v_G$  and  $param$  that give the lowest  $\bar{\epsilon}$ .
- Repeat process for a number of iterations, varying  $v_D$  and  $z_D$ .

We apply this method to the three geometric cases highlighted earlier - circular, hyperbolic, and parabolic, and estimate velocity correction factors for each case. Table 1 gives the parameters used for the generation of traveltime curves from a point diffractor geometry that we wish to compare with other geometries. The range of velocities covers the majority of the range of velocities of various subsurface materials, both natural and artificial (Davis and Annan, 1989; Jol, 2008). Additionally, since we are primarily interested in velocity changes, we have only allowed  $z_D$  to vary between 1.0 and 2.0 m depth, as with a smaller range the grid search will run faster. We generate 1000 different curves with which to run the inversion.

Parameter	Minimum	Maximum
$v_D$	$0.2c$	$0.8c$
$z_D$	1.0 m	2.0 m

Table 1. Range of parameters used to generate different zero-offset traveltimes curves in the geometric case of a single point diffractor buried in a homogeneous medium of velocity  $v_D$  at depth  $z_D$ .  $c$  is the propagation velocity of electromagnetic radiation in a vacuum.

### Circular geometry correction

The first case we discuss is the circular case presented in Figure 4b. The three geometric parameters that we would invert for would be medium velocity  $v_C$ , circle radius  $r$ , and depth of circle centre  $z_C$ . However, we note that in the limiting case of  $r \rightarrow 0$ , the normal raypath distance formula for a circular specular reflector (and hence the traveltimes formula) in Equation 5 approaches the normal raypath distance formula for a point diffractor (Equation 1). This makes sense for as  $r$  approaches zero, the circle is geometrically collapsing to a point, with  $z_C \rightarrow z_D$ .

It follows from this that if we allow  $r$  to vary in our grid search inversion in this circular case, it will almost tend to pick the smallest radius as this will give the best fit. We suspect that the differences in  $v_C$  and the diffractor velocity  $v_D$  that we want to estimate will be dependent on the radius of the circle, as in  $v_C(v_D, r)$ . Therefore, we modify our grid-search algorithm slightly. We run the grid-search algorithm for a number of fixed values of  $r$ , and then use these to get an estimation of  $v_C$  as a function of  $v_D$  and  $r$ , representing our velocity correction factor. The ranges and step sizes used can be seen in Table 2. We define the depth parameter to be the top of the circle  $z_T$  instead of depth to the centre of the circle  $z_C$  because it is the point we want to compare directly with  $z_D$  as it lies at the apex of the specular reflector, as opposed to  $z_C$ , which has no physical meaning in the reflection geometry.

Parameter	Minimum	Maximum	Step Size	No.
$v_C$	$0.1c$	$0.8c$	$0.01c$	71
$z_T$	0.5 m	2.5 m	0.1 m	21
$r$	0.5 m	5.0 m	0.5 m	10

Table 2. Grid search parameters used in the circular geometry case.  $c$  is the propagation velocity of electromagnetic radiation in a vacuum.

Figure 10 shows a plot of the the grid-search result values for velocity and depth vs. their respective counterparts in the input diffractor geometry case. The results for three particular radii are shown. Figure 11 shows the residual errors associated with the two parameters inverted for ( $v_C$  and  $z_T$ ). Figure 12 shows a similar plot to that in Figure 10, but with lines of best fit plotted over the data, and the equations of best fit displayed.

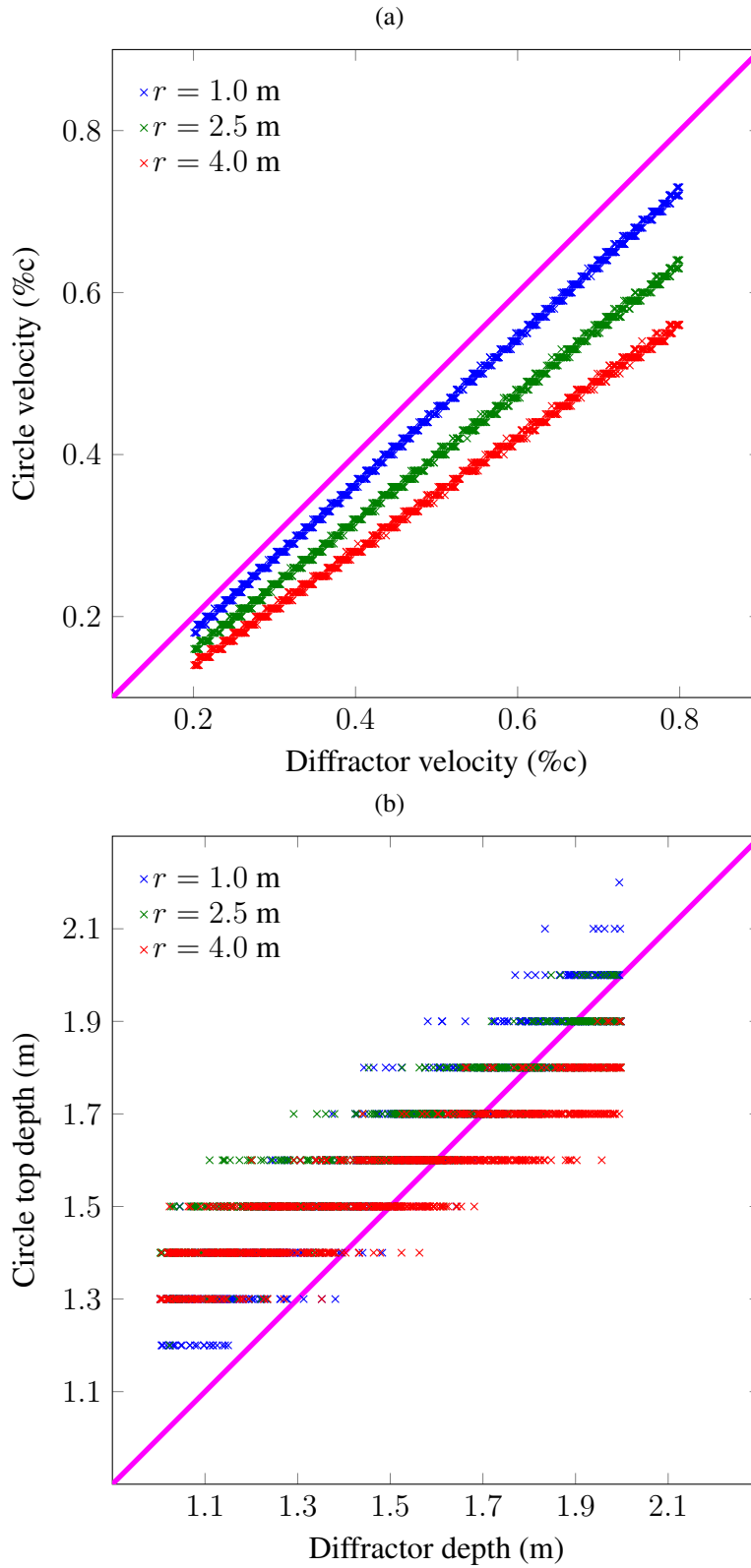


FIG. 10. Grid search inversion results for medium velocity with circular geometry vs. medium velocity with diffractor geometry (a) and depth to top of circular reflector vs. diffractor depth (b). The magenta lines represent 1-1 velocity and depth lines respectively.

Examining Figure 10a, we see that the best-fitting velocity in a circular reflector geometric case is always less than the diffractor velocity, which is expected. The relationship also appears to be strongly linear for each case of a constant non-zero  $r$ . Also, with a larger fixed radius, the relationship between  $v_C$  and  $v_D$  diverges more significantly from a 1-1 slope, especially at larger diffractor velocities. Again, this makes sense, as a larger radius represents a large deviation from a diffractor geometrically, translating to a larger discrepancy in velocity. In contrast, looking at the depth comparison in Figure 10b we observe a fairly significant range of results for top of circle depth to diffractor depth. We surmise that this is due to two reasons: 1) Our step size for circle top depths in the grid search inversion is too coarse which is visible in the discretization of the output  $z_T$  values in figure 10b, and 2) because we fix values of  $r$ , we introduce a non-unique tradeoff between circle top depth and radius. However, since we are primarily interested in the velocity relationship, this is of little concern.

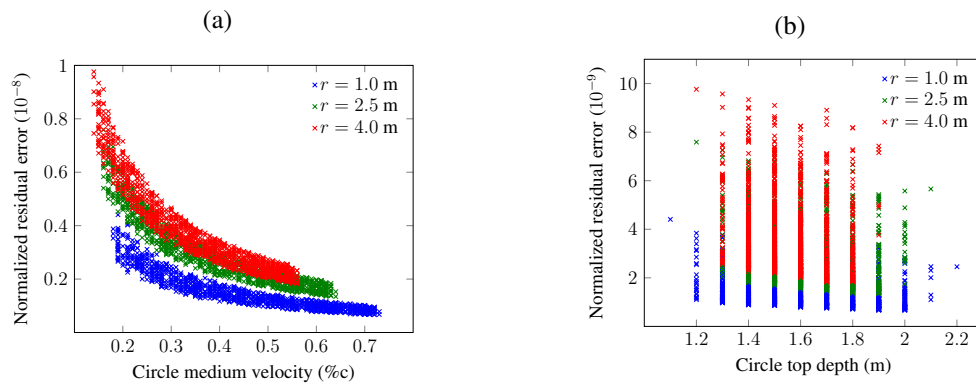


FIG. 11. error in grid search inversion results for two parameters in the circular reflector geometry case: medium velocity (a) and depth to top of circle (b) respectively.

In Figure 11 we see that relative error in the inversion decreases with faster medium velocities, and deeper circle top depths. also, a decrease in circle radius results in lower error - an explanation for which has been previously mentioned. the strongly correlated exponential decay in error with higher velocity in Figure 11a is interesting, and is likely related to the fact that faster velocities will generally generate flatter-shaped hyperbolic shapes in zero-offset traveltime data in both the diffractor and circular geometries. thus, it should be easier to find a velocities that can fit both traveltime curves with lower error.

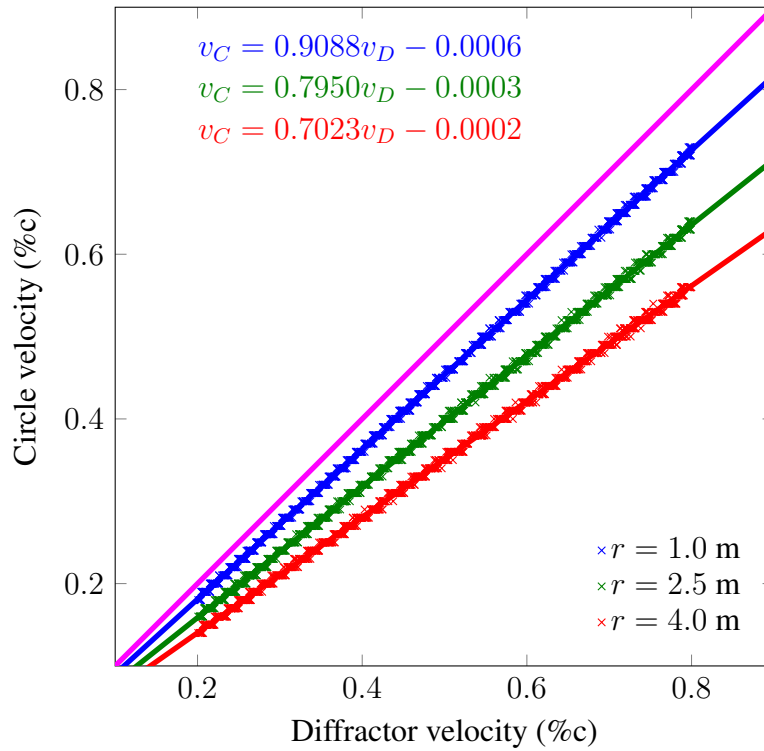


FIG. 12. same plot of  $v_C$  vs.  $v_D$  as shown in figure 10a with a line of best fit plotted over the inverted results for each sample radius. the equations of best fit for each of the sample radii are displayed in the same colour at the top-left of the plot. the magenta line represents a 1-1 velocity line.

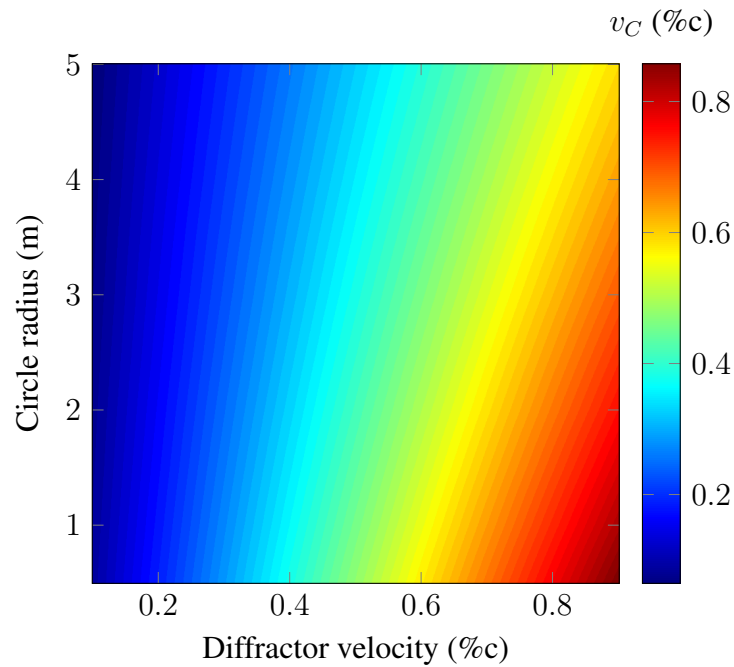


FIG. 13. surface showing  $v_C$  (color) as a function of  $v_D$  (x-axis) and  $r$  (y-axis).

we calculated the lines of best fit for velocity inversion results such as those displayed in Figure 10a, to get a different  $v_c(v_d)$  for each different  $r$  value in the range listed in table 2. Figure 12 illustrates an example of three such lines and their respective equations. using these relationships, we extended the velocity correction function to be in terms of both  $v_d$  and  $r$  by plotting the lines of best fit as data points on an  $v_D - r$  grid along horizontal lines of constant  $r$ . then we interpreted the grid over the entire parameter space. the result of this is shown in Figure 13, where the z-value (color) is  $v_C$  as a percentage of  $c$ . we note the extensions of the results seen in Figure 12, namely that  $v_C$  depends less on  $r$  as the diffractor velocity gets small, and diverges more at higher values of  $v_D$ .

The result in Figure 13 requires only that we have some knowledge of the scale (radius) of the image targets in order to be useful. In order to use the correction factor in imaging where we suspect circular geometry, what we would do is first figure out the value of  $v_D$  for a particular diffractor which can be done by collapsing the diffraction or by hyperbolic-curve fitting. Next, based on our estimate of scale we use the surface in Figure 13 to get a  $v_C$  that we then use to image the dataset. For the hyperbolic and parabolic reflector geometry cases, our methodology is much the same as for the circular case.

### Hyperbolic geometry correction

The next geometric case we consider is the hyperbolic reflector geometry case presented in Figure 5b. Unlike the circular case where radius  $r$  biased the inversion results, we do not have any one single parameter that would do the same. The only exceptions would be a very large  $a$  and/or very small  $b$ , which would geometrically cause the hyperbola to approach a near vertical shape, with its apex  $v_H$  acting in a similar manner to a point diffractor. The parameter ranges used in the grid search (table 3) avoid both of the situations, and instead of the circular case where  $v_C$  was a function of two parameters ( $v_D$  and  $r$ ), we want to find  $v_H$  only in terms of diffractor velocity. Similar to the circular case, we invert in terms of the apex of the hyperbola  $z_T$  instead of its "centre"  $z_H$ .

Parameter	Minimum	Maximum	Step Size	No.
$v_H$	$0.1c$	$0.8c$	$0.01c$	71
$z_T$	0.5 m	2.5 m	0.1 m	21
$a$	0.5	4.5	1.0	5
$b$	0.5	4.5	1.0	5

Table 3. Grid search parameters used in the hyperbolic geometry case.  $c$  is the propagation velocity of electromagnetic radiation in a vacuum.

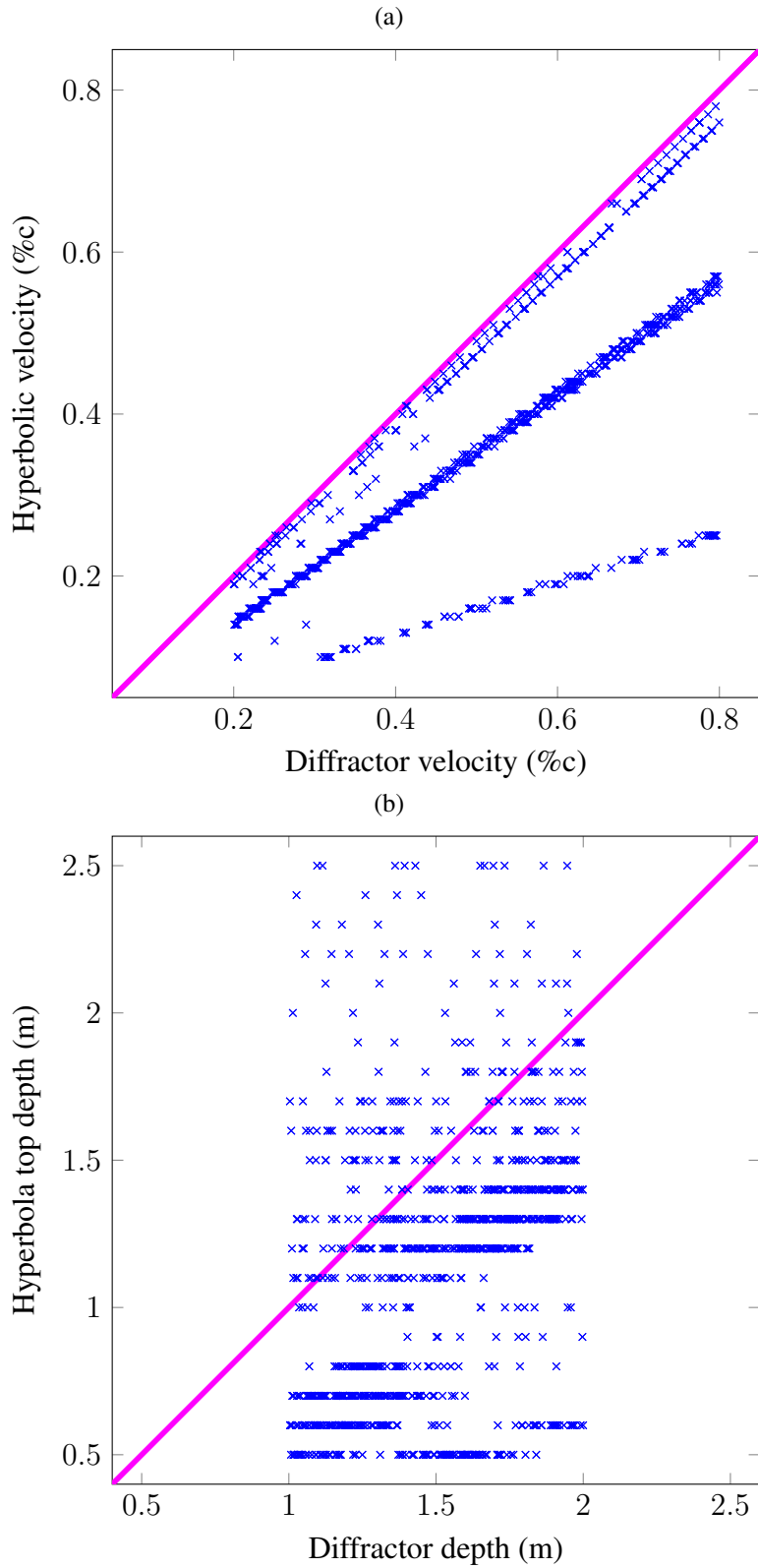


FIG. 14. Grid search inversion results for medium velocity with parabolic geometry vs. medium velocity with diffractor geometry (a) and parabola vertex depth vs. diffractor depth (b). The magenta lines represent 1-1 velocity and depth lines respectively.

In Figure 14a, we see again that the best-fitting velocity in a hyperbolic reflector case is always less than the diffractor velocity. There also appears to be linear relationships, with points clustering on several trajectories. Since we did not fix  $a$  or  $b$ , we assume that the velocities cluster based on the relationship between those parameters. In Figure 14b we observe a fairly significant spread of possible best-fitting hyperbola apex depths, more so than in the circular case (Figure 10b). Also, the majority of inverted depths are less than the diffractor depths. Again, this is likely due to a trade-off between depth ( $z_H$  or  $z_T$ ) and  $a$  and  $b$ .

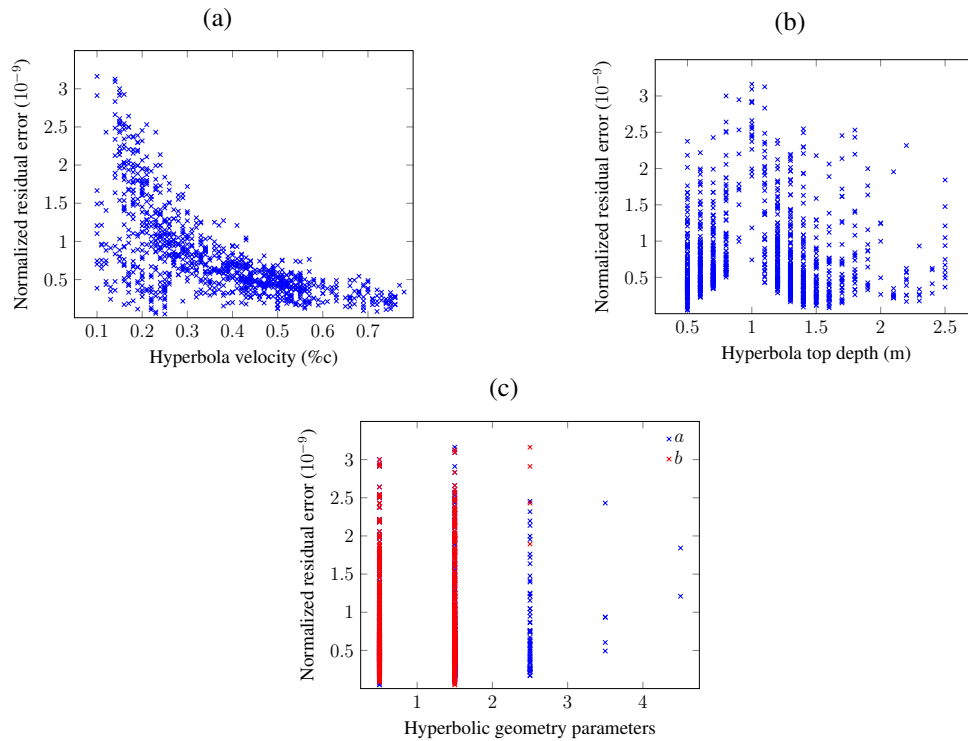


FIG. 15. error in grid search inversion results for two parameters in the circular reflector geometry case: medium velocity (a) and depth to top of circle (b) respectively.

in Figure 15b we see that relative error in the inversion decreases with faster medium velocities ( $v_H$ ) in a similar manner to the circular case. We see little change in error with changes in hyperbola top depth, with overall absolute errors being very small (Figure 15b). In Figure 15c, we notice an important relationship between  $a$  and  $b$  in that  $b$  values tend to be lower than  $a$  values. Also, errors are relatively small in absolute terms. Finally, we note using quite a coarse range for these parameters, and very few of best-fitting  $a$ 's and  $b$ 's tend to be greater than 3. In the future, we need to upsample our parameter space for  $a$  and  $b$  as well as shift it to lower overall values.

As we do not have a grasp on the geometric trade-offs between the geometric parameters  $a$  and  $b$ , we have not yet developed a velocity correction factor for the hyperbolic case.

## Parabolic geometry correction

The final case we discuss is the parabolic case presented in Figure 6b. The three parameters that we would invert for would be medium velocity  $v_P$ , curvature parameter  $p$ , and parabola vertex depth  $z_P$ . However, we note that in the limiting case that  $p \rightarrow 0$ , the normal raypath distance formula for a parabolic specular reflector (and hence the travel-time formula) in equation 19 is equal to zero at  $x = 0$ , and tends to a very large value with non-zero  $x$  values. This is approximately equivalent (geometrically) to the point diffractor case.

Similar to the circular case with  $r$ , if we allow  $p$  to vary in our grid search inversion in this parabolic case, it will almost tend to pick the smallest value as we would expect this to give the best fit as it matches the diffractor geometry the closest. Similarly again, we write a relationship for parabolic reflector velocity as a function of diffractor velocity and curvature parameter  $p$  as in  $v_C(v_D, p)$ . We run the gridsearch algorithm for a number of fixed values of  $p$ , and then use these to get an estimation of  $v_P$  as a function of  $v_D$  and  $p$ , representing our velocity correction factor. The ranges and step sizes used can be seen in Table 4.

Parameter	Minimum	Maximum	Step Size	No.
$v_P$	$0.1c$	$0.8c$	$0.01c$	71
$z_T$	0.5 m	2.5 m	0.1 m	21
$p$	0.5	4.5	0.5	9

Table 4. Grid search parameters used in the parabolic geometry case.  $c$  is the propagation velocity of electromagnetic radiation in a vacuum.

Figure 16 shows a plot of the the grid-search result values for velocity and depth vs. their respective counterparts in the input diffractor geometry case. The results for three particular  $p$ -values are shown. Figure 17 shows the residual errors associated with the two parameters inverted for ( $v_P$  and  $z_T$ ). Figure 18 shows a similar plot to that in Figure 16, but with lines of best fit plotted over the data, and the equations of best fit displayed.

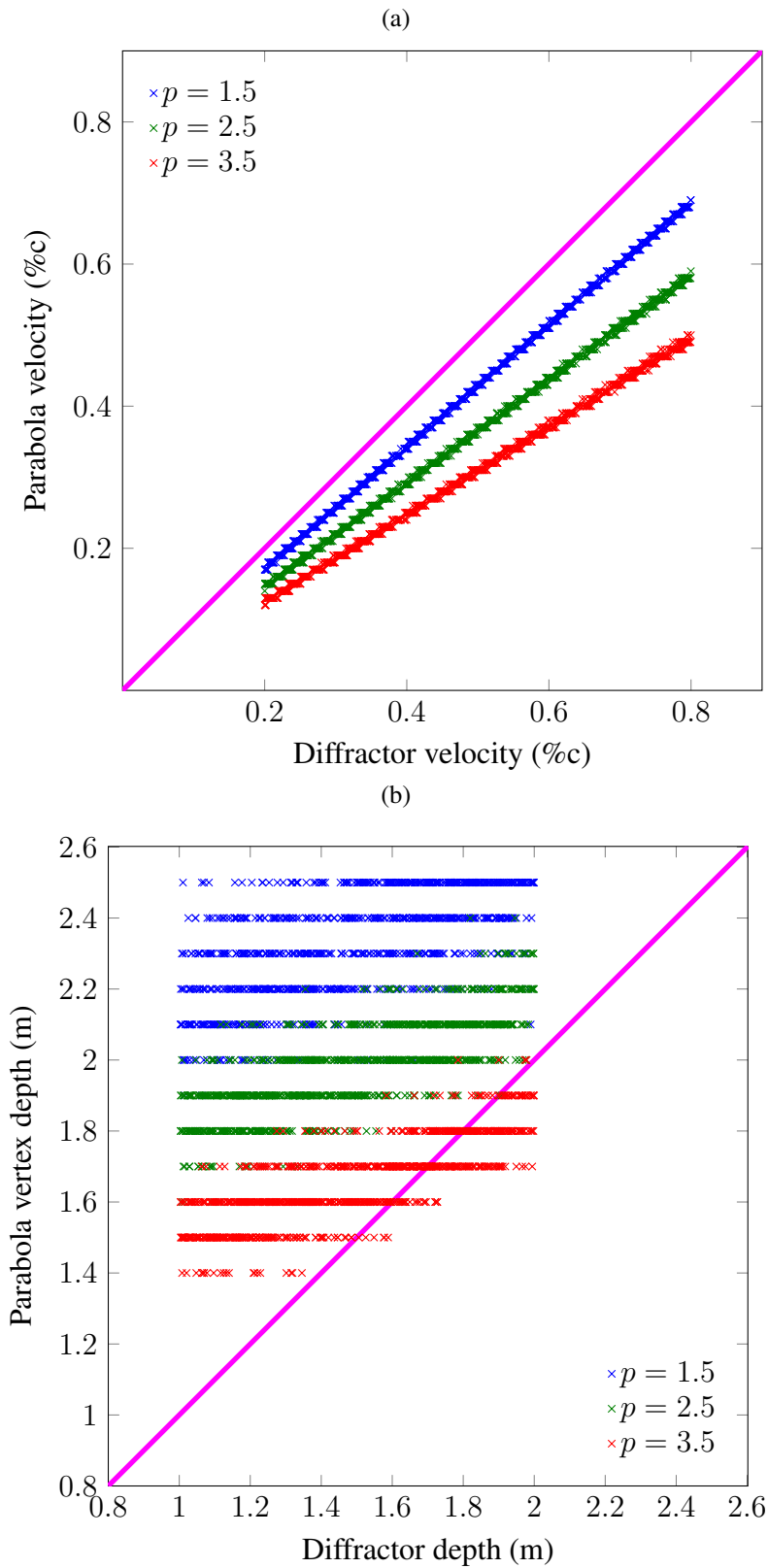


FIG. 16. Grid search inversion results for medium velocity with parabolic geometry vs. medium velocity with diffractor geometry (a) and parabola vertex depth vs. diffractor depth (b). The magenta lines represent 1-1 velocity and depth lines respectively.

Examining Figure 16a, we see again that the best-fitting velocity is always less than the diffractor velocity. The relationship again appears to be strongly linear for each case of a constant  $p$ . Also, with a larger  $p$  value, the relationship between  $v_P$  and  $v_D$  diverges more significantly from a 1-1 slope, especially at larger diffractor velocities. This is explained as a larger  $p$  represents a large deviation from a diffractor geometrically, translating to a larger discrepancy in velocity. In contrast,

Figure 16b illustrates a poor correlation between diffractor depth and parabola vertex depth. We notice that on the whole, the parabola vertices ( $z_P$ ) lie deeper than their corresponding diffractor depths. Also, as  $p$  decreases in value, the vertex depth increases relative to the diffractor depth in a fairly defined way. Further analysis is required to examine this relationship in more detail.

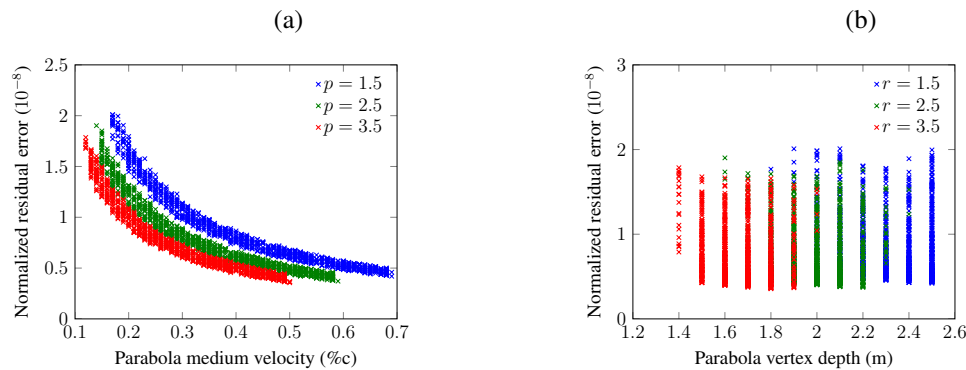


FIG. 17. error in grid search inversion results for two parameters in the circular reflector geometry case: medium velocity (a) and depth to top of circle (b) respectively.

In Figure 17a we see that relative error in the inversion decreases with faster medium velocities in a similar pattern to the circular and hyperbolic cases. There is no noticeable change in error with varying vertex depths (Figure 17b). As the error remains relatively constant across  $p$ -values and vertex depths, we surmise that there must be a poorly constrained trade off between depth and  $p$ -value that still gives the most "accurate" inversion result

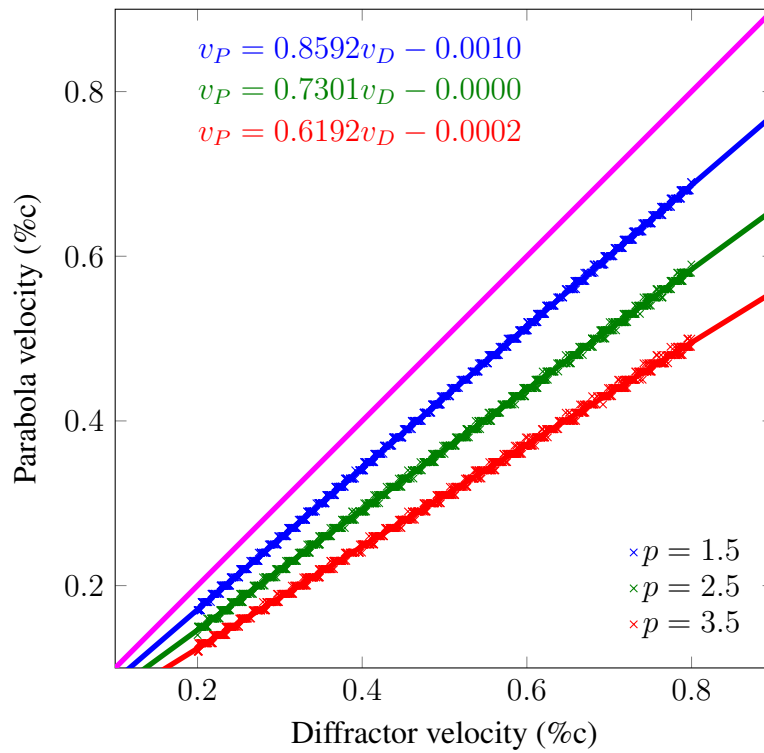


FIG. 18. same plot of  $v_c$  vs.  $v_d$  as shown in Figure 16a with a line of best fit plotted over the inverted results for each sample radius. the equations of best fit for each of the sample radii are displayed in the same colour at the top-left of the plot. the magenta line represents a 1-1 velocity line.

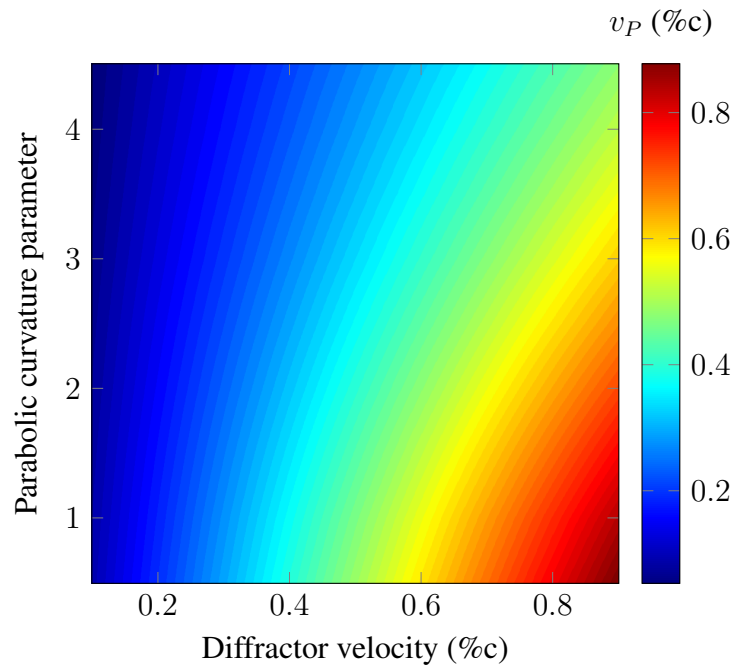


FIG. 19. surface showing  $v_P$  (color) as a function of  $v_d$  (x-axis) and  $r$  (y-axis).

We develop a velocity correction factor in the parabolic case similar to that in the circular case of  $v_P(v_D, p)$ , however this time our geometric variable is  $p$  instead of  $r$ . Figure 18 illustrates an example of the linear relationships between  $v_P$  and  $v_D$  for constant values of  $p$ . Figure 19 gives a surface representing our velocity correction function  $v_P(v_D, p)$  for the parabolic geometry case. Comparing with the circular velocity correction function in Figure 13, we see an even larger deviation of  $v_P$  from  $v_D$  at larger  $p$  values. For very large  $p$  values the differences in velocities approach 50%, which is significant enough to warrant applying the velocity correction where parabolic geometry is suspected. In order for the result in Figure 19 to be useful, we require an estimate of the parabolic curvature parameter  $p$ .

### HOUSTON COASTAL CENTER EXAMPLE

As mentioned earlier, our motivation for deriving the correction factors is related to a georadar dataset collected at the Houston Coastal Center over a series of circular-shaped culverts. In Smith et al. (2014) we fitted diffraction hyperbolae to the processed 2D Culvert Line in order to determine diffractor velocities. The average diffractor velocity for the four culvert reflection signatures was found to be about  $0.425c$ . Assuming an approximate circle radius of 1.5 m, the circular velocity correction function in Figure 13 is

$$v_C(r, v_D)|_{r=1.5} = 0.864v_D. \quad (20)$$

As  $v_D$  is about  $0.425c$  in this case as determined from diffraction hyperbola fitting, we calculate  $v_C$  to be about  $0.368c$ . We generated constant velocity models with both the diffractor and circular-corrected velocities models and migrated using zero-offset Gazdag migration and shot-record Gazdag PSDM (Gazdag, 1978; Smith et al., 2014). Figure 20 gives a comparison between the two PSDM sections, one migrated using the diffractor velocity (20a) and the other using the geometrically-correction velocity (20b).

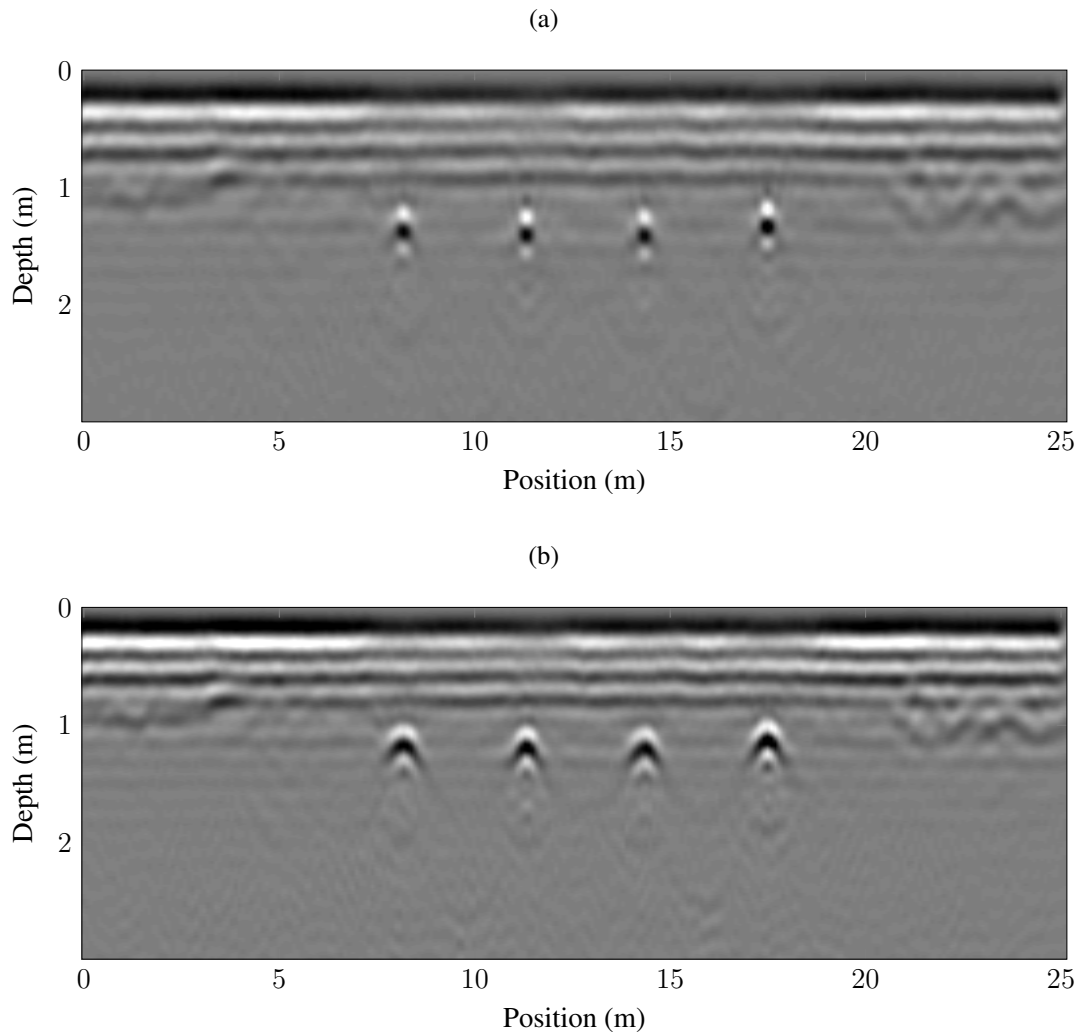


FIG. 20. Shot-record Gazdag PSDM sections of the Culvert Line from the Houston Coastal Center. (a) Constant velocity medium of  $0.425c$ , determined from diffraction hyperbola fitting. (b) Velocity model corrected for circular geometry, constant velocity of  $0.368c$ . Both images are 3x vertically exaggerated (Smith et al., 2014).

We observe that the diffraction hyperbola-fitted velocities collapse the energy onto points, which is what we would expect that algorithm to do (Figure 20a). We observe that the velocity-corrected image appears clearer and more focused, especially at shallow depths. This indicates that the geometrically-corrected value is giving us a better velocity estimate.

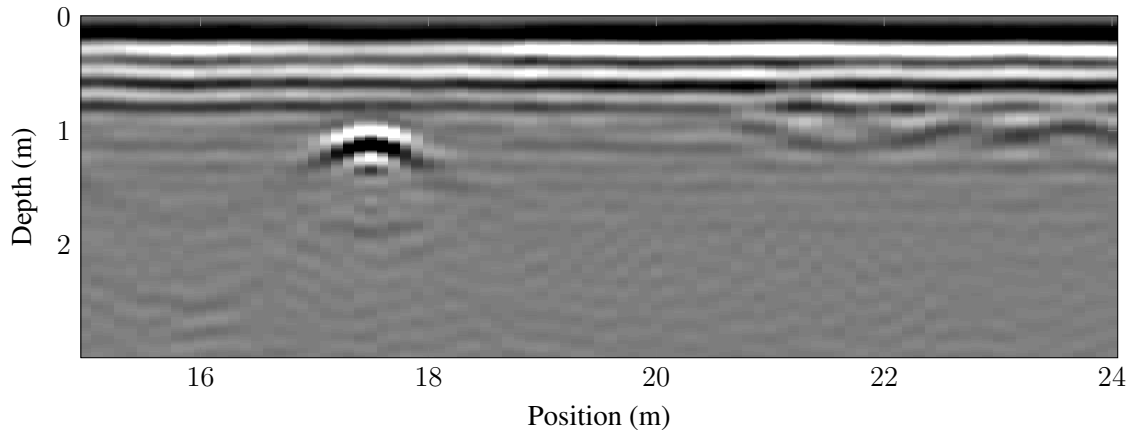


FIG. 21. Portion of the shot-record Gazdag PSDM section from Figure 20b displayed at a 1-1 scale.

Figure 21 contains a portion of the image generated with shot-record Gazdag PSDM displayed at a 1-1 scale. We notice that although the image shows us a curved culvert, it does not appear as curved as the actual culvert (Figure 1). Although the geometry-corrected velocity is better than the diffractor velocity it is still higher than the true medium velocity, as the final image is "overmigrated" in the sense that the culvert curvature is less than that of a circle. This is possibly because the velocity corrections described earlier were derived for true zero-offset acquisition geometry, whereas the Houston Coastal Center data is bistatic with a slight fixed offset. Our choice of  $r$  may also be incorrect.

## CONCLUSIONS

The goal of this work was to address the ambiguity between velocities obtained through diffraction hyperbola fitting on fixed-offset data and non-point diffractor geometry in the subsurface. We derived zero-offset traveltime curves for four subsurface geometries: point diffractor, circular interface, hyperbolic interface, and parabolic interface. Using a sample of diffractors and depths, we inverted for the best fitting geometric parameters and medium velocities that would best match the diffraction curves using a simple grid-search method. This was done to develop a relationship between observed diffractor velocity and true velocity to be used as a correction factor in velocity model building and imaging. In the circular and parabolic cases, we found a linear relationship present between velocities when we fixed a geometric parameter. This allows us to apply a velocity correction with only the assumption of the scale of the features. In the hyperbolic case, there is a trade off between two geometric parameters which prevented the estimation of a correction factor, however we did observe linear relationships in a velocity comparison plot.

We applied a geometry correction to the velocities obtained from diffraction hyperbola fitting of a georadar survey acquired at the Houston Coastal Center over a series of culverts. Application of the correction gives a more accurate image than migrating using the diffractor velocity, however we note that improvements to the correction still need to be made to further improve the final image result.

## **Future work**

The results from the Houston Coastal Center show us that we need to extend our travel-time curve derivation and velocity correction estimation for the various geometric cases to a general fixed-offset case, introducing a new offset parameter. We also would like to improve the efficiency of our inversion algorithm, requiring a non-linear inversion technique to do so. The Houston Coastal Center provides us with an excellent dataset with which we can do further testing.

## **ACKNOWLEDGEMENTS**

We thank the sponsors of CREWES for their support. We gratefully acknowledge support from NSERC (Natural Science and Engineering Research Council of Canada) through the grant CRDPJ 379744-08. We would also like to thank Rob Stewart and the University of Houston for providing the Houston Coastal Center georadar dataset.

## REFERENCES

- Biondi, B., 2009a, Measuring image focusing for velocity analysis: SEP Research Report, **138**.
- Biondi, B., 2009b, Measuring velocity from zero-offset data by image focusing analysis: SEP Research Report, **139**.
- Davis, J., and Annan, A., 1989, Ground-penetrating radar for high-resolution mapping of soil and rock stratigraphy: *Geophysical prospecting*, **37**, No. 5, 531–551.
- de Figueiredo, J., Oliveira, F., Esmi, E., Freitas, L., Schleicher, J., Novais, A., Sussner, P., and Green, S., 2013, Automatic detection and imaging of diffraction points using pattern recognition: *Geophysical Prospecting*, **61**, No. s1, 368–379.
- de Figueiredo, J. S., Oliveira, F., Esmi, E., Freitas, L., Green, S., Novais, A., and Schleicher, J., 2011, Diffraction imaging point of common-offset gather: Gpr data example, *in* 12th International Congress of the Brazilian Geophysical Society.
- Forte, E., Dossi, M., Pipan, M., and Colucci, R. R., 2014, Velocity analysis from common offset gpr data inversion: theory and application to synthetic and real data: *Geophysical Journal International*, **197**, 1471–1483.
- Gazdag, J., 1978, Wave equation migration with the phase-shift method: *Geophysics*, **43**, No. 7, 1342–1351.
- Grasmueck, M., Weger, R., and Horstmeyer, H., 2005, Full-resolution 3D GPR imaging: *Geophysics*, **70**, No. 1, K12–K19.
- Jol, H. M., 2008, *Ground penetrating radar theory and applications*: Elsevier.
- Novais, A., Costa, J., and Schleicher, J., 2008, GPR velocity determination by image-wave remigration: *Journal of Applied Geophysics*, **65**, 65–72.
- Smith, A. D., Ferguson, R. J., and Stewart, R. R., 2014, *Georadar processing and imaging with Gabor deconvolution - Houston Coastal Center: CREWES Research Report*, **26**.
- Yilmaz, Ö., 2001, *Seismic data analysis, vol. 1*: Society of Exploration Geophysicists Tulsa.